NJC

Accepted Manuscript

This is an *Accepted Manuscript*, which has been through the Royal Society of Chemistry peer review process and has been accepted for publication.

Accepted Manuscripts are published online shortly after acceptance, before technical editing, formatting and proof reading. Using this free service, authors can make their results available to the community, in citable form, before we publish the edited article. We will replace this *Accepted Manuscript* with the edited and formatted *Advance Article* as soon as it is available.

You can find more information about *Accepted Manuscripts* in the Information for Authors.

Please note that technical editing may introduce minor changes to the text and/or graphics, which may alter content. The journal's standard Terms & Conditions and the Ethical guidelines still apply. In no event shall the Royal Society of Chemistry be held responsible for any errors or omissions in this *Accepted Manuscript* or any consequences arising from the use of any information it contains.

ROYAL SOCIETY OF CHEMISTRY

www.rsc.org/njc

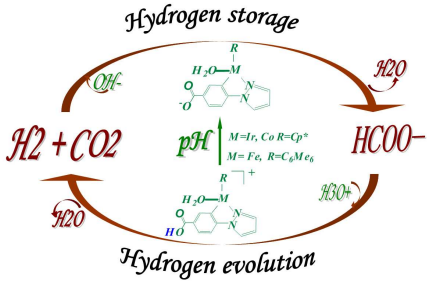

Our theoretical results will facilitate mechanistic understanding of growing interesting sustainable H_2 storage/delivery in homogeneous catalysis.

Mechanistic Studies on the pH-Controllable Interconversion between Hydrogen and Formic Acid in Water: A DFT Insights

Dandan Zhang, Xiankai Chen, Huiling Liu* and Xuri Huang

Institute of Theoretical Chemistry, Jilin University, Changchun, 130023, China.

*E-mail: huiling@jlu.edu.cn

Abstract

A complete reaction mechanism for interconversion between hydrogen and formic acid catalyzed by [C,N] cyclometallated organoiridium complex, $[Ir^{III}(Cp^*)(4\text{-}(1H\text{-pyrazol-1-yl-k}N^2)\text{benzoic acid-k}C^3)(H_2O)]_2\cdot SO_4$, i.e. $[\mathbf{1\text{-}Ir}]_2\cdot SO_4$ has been revealed by density functional theory (DFT) calculations. For both the hydrogen storage catalytic cycle I and hydrogen evolution catalytic cycle II, the detailed reaction profiles with the key transition states and intermediates are revealed. Catalytic cycle I show that the dihydrogen heterolysis facilitated by OH^- gives the considerable stable iridium hydride intermediate **M-4** followed by an outer-sphere hydrogen transfer to afford a metal-formate complex **M-6**. Upon the increasing of pH, catalytic cycle II occurs via the generation of the metal-formate complex **M-10** followed by the outer-sphere *β*-H elimination to form a metal-hydride complex **M-12**, which is subsequently protonated by the hydrated proton H_3O^+ to afford dihydrogen. The decomposition of bicarbonate and the *β*-hydride elimination of formate are

believed to be the rate-determining steps for cycle I and II, respectively. The acid-base equilibrium between the hydroxy and oxyanion form on the catalyst [C, N] ligand has a considerable influence on the catalytic hydrogen transfer. Our studies are well in agreement with experimental results. Remarkablely, new theoretical designed low-cost cobalt (III) complex as promising catalyst exhibit the catalytic activity for the interconversion between hydrogen and formic acid.

Keywords: DFT mechanism study, hydrogen storage, hydrogen evolution, formic acid, CO_2

1. Introduction

Hydrogen as a clean and renewable energy feedstock is extremely important, especially for fuel-cell technology with a numerous advantages over fossil fuels.[1] However, the practical application of hydrogen as a transportation fuel is limited mainly because conventional hydrogen-storage methods (high-pressure gas containers or cryogenic liquid/gas containers) have weight and safety issues. Considering the low potential risk and capital investment, the promising hydrogen storage techniques gradually relay on liquid-phase chemical hydrogen storage materials. Thus, a large number of researches are being conducted to develop the new effective hydrogen (H_2) storage/generation materials. Formic acid (FA) containing 4.4 wt% of hydrogen as nontoxicity and excellent stability liquid-phase organic material at room temperature is largely compatible with the current transport infrastructure and has recently attracted tremendous research interests.[2] In addition, because of the continually rising levels of CO_2 in the atmosphere, the catalysis storage of H_2 in formic acid by

consuming the waste carbon dioxide (CO_2) from industry has also been current and important topic.[3] Therefore, the combination between carbon dioxide and formic acid as a hydrogen storage system is an excellent concept, in which the reversible cycle consists of selective decomposition of formic acid to H_2 and CO_2 (hydrogen supply) and reduction of CO_2 to formic acid by H_2 (hydrogen storage).

For storing hydrogen in FA by reduction of carbon dioxide, numbers of homogeneous transition-metal Cp*-catalysts[4] (Cp*= pentamethylcyclopentanyl) or pincer-catalysts[5] had been utilized in economically desirable and environmentally benign water solvent. Yuichiro H. and co-workers[6] reported hydrogenation of CO_2 and hydrogen carbonate is catalyzed by half-sandwich complexes with 4,4′-dihydroxy-2,2′-bipyridine,[7] where the oxyanions generated from the phenol hydroxyl groups played significant roles in the electronic effect and polarity.[8] These protonic groups improve the catalytic activity by tuning the complexes' electronic properties upon deprotonation. Furthermore, the reverse reaction, i.e., decomposition of FA to CO_2 and H_2 has also been widely investigated by experimental and theoretical methods.[2a, 9] However, little studies have been achieved for the effective controlled interconversion of CO_2 and formic acid under mild conditions in water, which is vital to the pragmatic applying in industry.[10] One key question is that the formic acid decomposes to CO_2 and H_2 once the formic acid is formed and the gas pressure is reduced, because catalysts for hydrogen evolution reaction are also catalysts for the hydrogen storage reaction. Recently, Fukuzumi and coworkers reported a well-defined [C,N] cyclometalated iridium catalyst system capable of

interconversion between hydrogen and formic acid at ambient temperature and pressure.[11] The important is that the reversibility can be turned on or off by slightly adjusting the pH of the solution because the [C,N] cyclometalated catalyst [Cp*Ir(4-(1H-pyrazol-1-yl-κN_2)benzoic acid-κC^3)(H_2O)]$_2$ has the proton-responsive [12] (i.e., pH-responsive) benzoic acid functional group. The strong pH influence is attributed to the acid-base equilibrium of the carboxylic, which tunes the catalyst structure between the hydroxy and oxyanion form. This catalytic system has the highly catalytic performance and no CO was produced during the decomposition reaction.

In this work, for Fukuzumi and coworkers's CO_2–FA hydrogen-storage catalytic system, we investigate the underlying chemical transformations mechanism with the key intermediates and transition states on the basis of DFT calculations. DFT has proven to be an extremely powerful tool for the characterization of unknown pathways and the interpretation of the reaction process that are not fully understood.[13] As shown in scheme 1, the benzoic acid ligand of complex **Ir-1** dissociates the labile proton (in blue) to form benzoate complex **Ir-2** in the slightly basic environment. Therefore, based on deprotonation/protonation equilibrium between active catalysts **Ir-1** and **Ir-2** as the pH increases/decrease during the reaction, hydrogen storage and evolution catalyzed by **Ir-2** and **Ir-1** will occur, respectively. The proton responsive ligand may change the catalytic activity of the corresponding catalyst at different pH conditions so that different rate-determining steps are possible to the forward and reverse reactions. Our study also focuses on potential roles of the hydroxyl anion in

basic solution, the hydrated proton in acid solution, and the [C, N] cyclometalated ligand in catalytic process.[14]

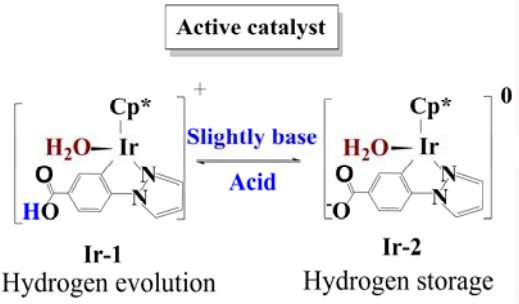

Scheme 1. Interconversion between hydrogen storage active catalyst **Ir-2** and hydrogen evolution active catalyst **Ir-1**.

In addition, it is serious concern of current catalytic reactions that the highly active catalysts are restricted to the precious metals complexes. Although some first-row metals Fe[15] and Co[16] complexes have become competitive with many known precious-metal catalysts for the hydrogenation of CO_2, making the successively substantial efforts are still significantly necessary because of their potential activities and relatively low costs.[4a, 16-17] Therefore, we computationally design two similar catalysts **Fe-1** and **Co-1** as candidates, which are expected to be promising catalysts. Our insights into the cobalt and iron catalyst should be important to the rational development of low-cost catalyst that can catalyze the interconversion between formic acid and carbon dioxide.

2. Computational methods

All calculations were performed by using the Gaussian 09 program package.[18] The M06[19] functional was used due to its good predictions for both geometric

parameters and reaction energies in organometallic compounds. The structures studied in this paper were optimized in water solvent by using SMD[20] (solvation model density), that is a universal solvation model based on the polarized continuous quantum mechanical charge density of the solute. Geometric optimization basis set is BSI that represents the basis set combination of SDD[21] for metal atoms (Ir, Co, and Fe) and the all-electron 6-31G(d,p) for N, O, H and C atoms. Each stationary point was classified as a minimum (no imaginary frequency) or a transition state (only one imaginary frequency) by analytical calculation of the frequencies at the M06/BSI (SMD, water) level. In addition, IRC[22] (intrinsic reaction coordinate) calculation at the M06/BSI level was performed to confirm the correct connections between a transition state and its forward and backward minima. Moreover, full vibrational and thermochemical analysis of these stationary structures were performed on optimized structures under T = 298.15 K and 1 atom pressure. Based on the M06/BSI (SMD, water) geometries, the energy of each species was refined by a single-point calculation at the M06/BSII (SMD, water) level (BSII denotes the basis set combination of SDD for Ir, Fe and Co atoms and the all-electron 6-311++G(d,p) for N, O, H and C atoms). Unless otherwise noted, the energies in this paper are Gibbs free energies ΔG at the M06/BSII (SMD, water) level in the singlet state. Some species has the more than one geometry, the most favorable one are used here. Because the reverse equation $H_3O^+ \rightleftharpoons H_2O + H^+$ exists in real water solution, we used the energy of H_3O^+ to calculate the protonation and deprotonation processes in the potential energy surfaces.

3. Results and Discussion

Herein, for both the hydrogen storage catalytic cycle I catalyzed by active catalyst **Ir-2** and hydrogen evolution catalytic cycle II catalyzed by active catalyst **Ir-1**, the detailed reaction profiles with the key transition states and intermediates are revealed. Because Ir, Fe, and Co complexes have similar catalytic reaction pathways, the mechanism illustrations are shown together (hydrogen storage and hydrogen evolution are in schemes 2 and 3, respectively). In section 3.1, we comparatively analyze the structures of catalysts **Ir-2**, **Co-2**, and **Fe-2**. The corresponding detailed free energy profiles of hydrogen storage and hydrogen evolution are discussed in section 3.2 and 3.3, respectively. In section 3.4, we consider the high-spin state cases of both Co and Fe models. The activation free energy barrier ($\Delta G^{\ddagger}$) is defined as free energy difference between the highest point and the forward lowest point in pathway given.

3.1 Structural comparison of catalysts Ir-2, Co-2, and Fe-2.

As shown in Figure 1, the optimized structure of **Ir-2** is given, where coordination bonds Ir-C, Ir-N, and Ir-O are 2.069 Å, 2.134 Å, and 2.342 Å, respectively. We designed the new catalyst **Co-2** by replacing the center Ir by Co, where the strained coordination structure is found, that is, Co-C, Co-N, and Co-O are 1.932 Å, 1.959 Å, and 2.036 Å, respectively. The catalyst **Fe-2** is given by replacing both center Ir and ligand Cp* ring by Fe and hexamethylbenzene, respectively. Likely, the coordination structure around Fe center is strained. The low-row metals both Fe

and Co have the less *d* electrons than Ir, which likely results in the stronger metal-ligand interactions in the new catalysts **Co-2** and **Fe-2**.

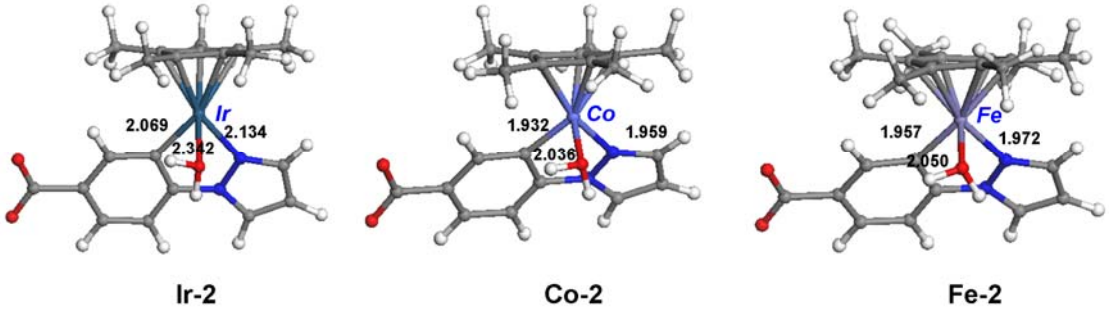

Figure 1. The optimized structures (bond length/Å) for three active catalysts **Ir-2**, **Co-2**, and **Fe-2**.

3.2 Hydrogen storage

For hydrogen storage catalytic cycle I catalyzed by **M-2** in slightly base solution, overall mechanism illustration is presented in scheme 2, the free energy profiles are shown in Figures 2, 5, and the corresponding key optimized structures are given in Figures 3, 4, and 6.

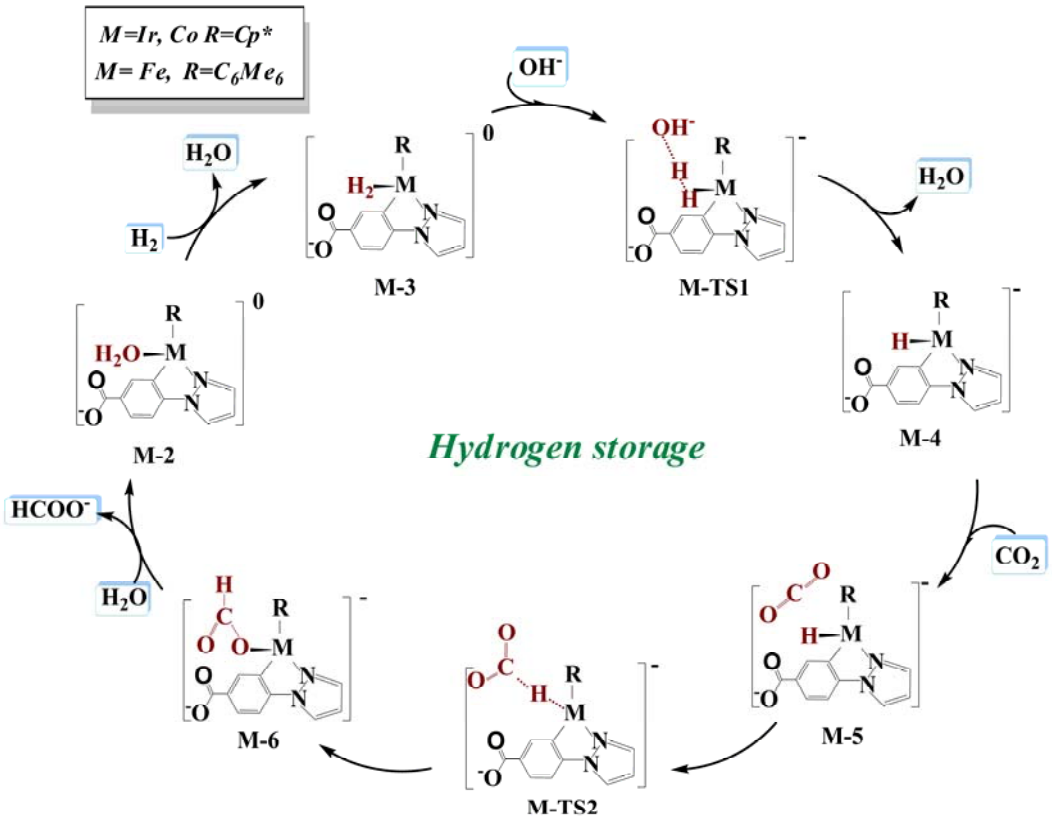

Scheme 2. Overall mechanism schematic illustration for the storage of dihydrongen into carbon dioxide to form formate catalyzed by **M-2** in slightly base solution (*Cycle I*).

3.2.1 Dihydrogen heterolysis

As shown in scheme 2, starting with the active catalyst **M-2**, a ligand exchange of H_2 for H_2O firstly occurs to give the dihydrogen complex **M-3**. This ligand exchange step is 2.5 kcal/mol downhill, 0.7 kcal/mol uphill, and 1.0 kcal/mol downhill for Ir, Co, and Fe, respectively, indicating easily ligand exchange process (see Figure 2). For the subsequent heterolysis cleavage of dihydrogen, we explored four possible transition states, of the most feasible is **Ir-TS1** with $\Delta G^{\ddagger} = 10.8$ kcal/mol. As shown in Figure 3, transition state **Ir-TS1** describes dihydrogen heterolysis with the outer-sphere aid of the free base anion OH^-. In transition state **Ir-TS1**, anion OH^- have

the stronger H-bond interaction with H1 than H2 ($d_{H1\text{-}OH^-}$=2.009Å *vs* $d_{H2\text{-}OH^-}$=2.139Å), which leads to the longer bond length of Ir-H1 bond than Ir-H2 bond ($d_{Ir\text{-}H1}$=1.737Å *vs* $d_{Ir\text{-}H2}$=1.728Å). Compared to H1-H2 bond ($d_{H1\text{-}H2}$=0.857Å) in intermediate **Ir-3,** the H1-H2 bond in **Ir-TS1** has been lengthened to 0.878 Å. For analogous transition states **Co-TS1** and **Fe-TS1**, the same structure features were found, but it is opposite to Ir model that Ir-H2 bond is longer than Ir-H1 bond. The activation barriers of transition states **Co-TS1** and **Fe-TS1** are 10.4 kcal/mol and 10.2 kcal/mol, respectively, which are slightly lower than that of transition state **Ir-TS1**. As shown in Figure 4, the other three reaction manners of the dihydrogen heterolysis are presented by transition states **H_2O-TS1**, **HO-TS1**, and **N-TS1**. The transition state **H_2O-TS1** describes the "proton relay" hydrogen transfer by both pendent base and water mediator, that is, H1 atom is transferred to O atom of water mediator while the H2 atom of water mediator is transferred to pendent base COO^- ($d_{H1\text{-}H2}$=1.001Å, $d_{H1\text{-}O}$=1.305Å, and $d_{H3\text{-}O}$=1.808Å) with the activation barrier of 21.4 kcal/mol. The transition state **HO-TS1** describes that the hydroxyl anion bonds to Ir accompanied with the breaking of Ir-N coordination bond ($d_{Ir\text{-}N}$=4.355Å) followed by the hydroxyl ligand abstracts a hydrogen of coordinated H_2, leading to the heterolysis of H_2 with the activation barrier of 14.4 kcal/mol. The transition state **N-TS1** describes direct heterolysis of dihydrogen by the participation of the Ir-N arm of [C, N] bidentate ligand, where hydrogen transfers ($d_{H1\text{-}N2}$=1.207Å) to N atom of the weaken Ir-N bond ($d_{Ir\text{-}N}$=2.441Å) with the activation barrier of 24.2 kcal/mol. It is obvious that these reaction manners corresponding to the heterolytic H_2 cleavage all have the relatively

highly activation barriers. The serious distorted structures of the [C,N] ligands may be the main reason of the highly activation barriers. The structural distortions of the [C,N] ligands are reflected not only by the cleavage of Ir-N bond (for **OH-TS1** and **N-TS1)** but also the existence of dihedral angles, 0.07°, 60.99°, and 10.07° for **H_2O-TS1**, **OH-TS1**, and **N-TS1**, respectively. After the dihydrogen heterolysis by the hydroxyl anion, the liberation of water molecule gives the considerable stable iridium hydride complex **M-4**, which is -34.6 kcal/mol (**Ir-4**), -28.3 kcal/mol (**Co-4**), and -22.3 kcal/mol (**Fe-4**) relative to the initial **Ir-1**, **Co-1**, and **Fe-1**, respectively. The iridium hydride complex **M-4** is lowest point in free energy profile of the hydrogen storage catalytic cycle, so it is extremely likely to be the resting sate in hydrogen storage cycle. This is in agreement with that species **Ir-4** has been easily detected in experiment. The metal-H species usually are proposed as the key intermediate in the storage of H_2 into CO_2 due to high reduction activity.

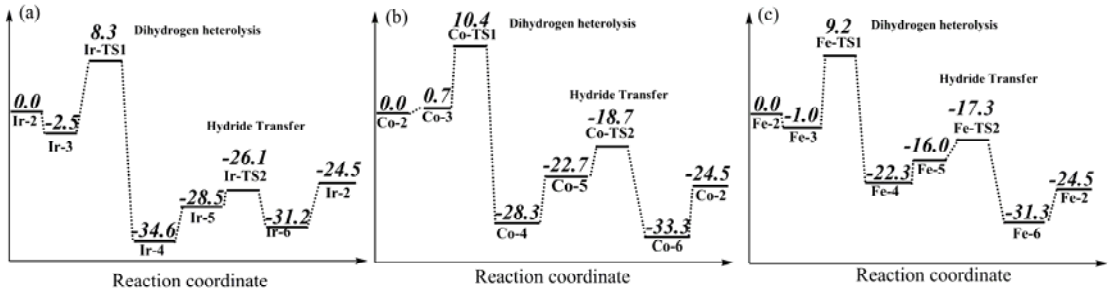

Figure 2. The free energy (italic numbers in kcal/mol) profiles for the hydrogen storage catalyzed by **Ir-2** (a), **Co-2** (b), and **Fe-2**(c).

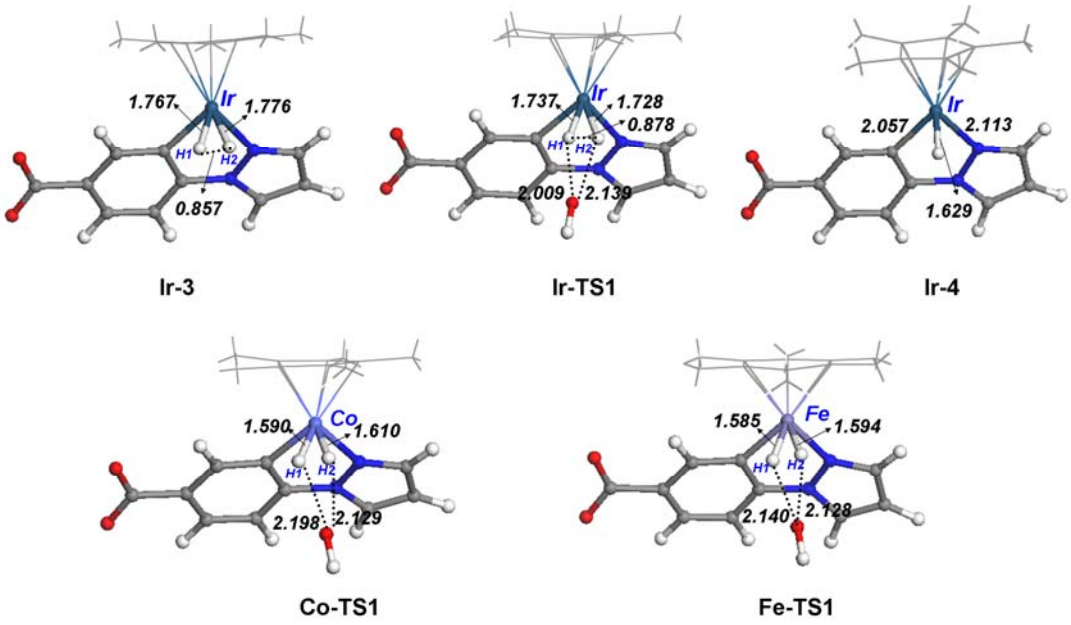

Figure 3. The optimized transition state structures (bond length/Å) involved in dihydrogen heterolysis in Figure 2.

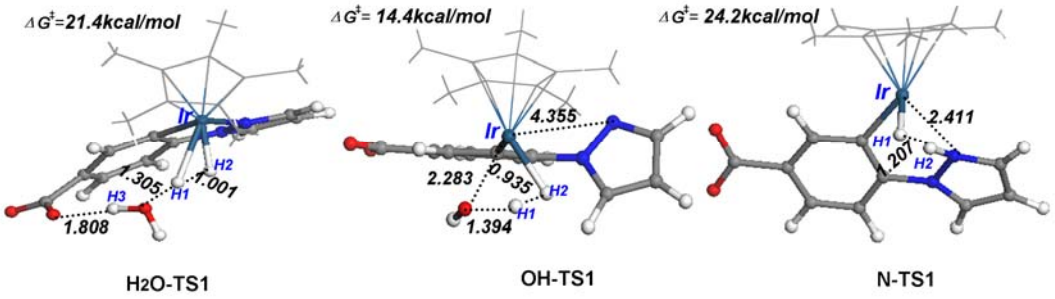

Figure 4. Others possible transition states (bond length/Å) involved in dihydrogen heterolysis.

For both the intermediate **Ir-3** and transition state **Ir-TS1** shown in Figure 2, we performed single-point calculations on the basis of various DFT functionals including M06-L, TPSS, PBE, M05-2X, B3PW91, and B3LYP. From the Table 1, it can be found that the free energy barriers ($\Delta G^{\ddagger}$) between **Ir-TS1** and **Ir-3** calculated by all functionals are close to that given by M06 except that the barriers by both B3PW91 and B3LYP are lightly higher, indicating the reliability of our computational method.

Table 1. The single-point calculations (in kcal/mol) for dihydrogen heterolysis activation barrier involving the intermediate **Ir-3** and transition state **Ir-TS1** in Figure 2 on the basis of various DFT functionals including M06, M06-L, TPSS, PBE, M05-2X, B3PW91, and B3LYP.

	M06	**M06-L**	**TPSS**	**PBE**	**M05-2X**	**B3pw91**	**B3LYP**
Ir-3	-2.5	-2.3	-2.1	-5.3	-1.2	-5.7	-3.8
Ir-TS1	8.3	8.7	10.5	5.7	9.6	7.9	10.2
$\Delta G^{\ddagger}$	10.8	11.0	12.6	11.0	10.8	13.6	14.0

As shown in Figure 5, when the pH is increased, the aqua complex **Ir-2** can release protons from the aqua ligand to form the corresponding hydroxo complex **Ir-2′**. In experiment, compared to the formation of **Ir-4** from **Ir-2** with H_2 in slightly base surrounding, it is slower that **Ir-4** comes from **Ir-2′** with H_2 under basic conditions. For complex **Ir-2**, the ligand exchange of H_2 for H_2O is exergonic by 2.5 kcal/mol. On the contrary, for complex **Ir-2′**, the ligand exchange of H_2 for $HO^{\delta-}$ is significantly endergonic by 13.8 kcal/mol. It is reasonable that the electronegativity $HO^{\delta-}$ is difficult to leave away from the positivity electricity iridium center. The hard decoordination of $HO^{\delta-}$ ligand directly leads to that transition state **Ir-TS1** has the 24.6 kcal/mol higher active barrier relative to **Ir-2′**. So our calculations suggest the slowly formation of **Ir-4** from **Ir-2′** is mainly ascribed to the strong coordination interaction between hydroxo ligand and iridium center in **Ir-2′**. It is satisfactory that the overall reaction process is thermodynamically 18.3 kcal/mol considerable

favorable. For the Co model, the barrier form **Co-2'** to **Co-TS1** is 24.2 kcal/mol, which is analogous to that of Ir model. However, the barriers form **Fe-2'**to **Fe-TS1** is higher, 27.8 kcal/mol, because the stronger Fe-OH coordination bond leads to the harder formation of intermediate **Fe-3**, so the higher barrier of transition state **Fe-TS1**.

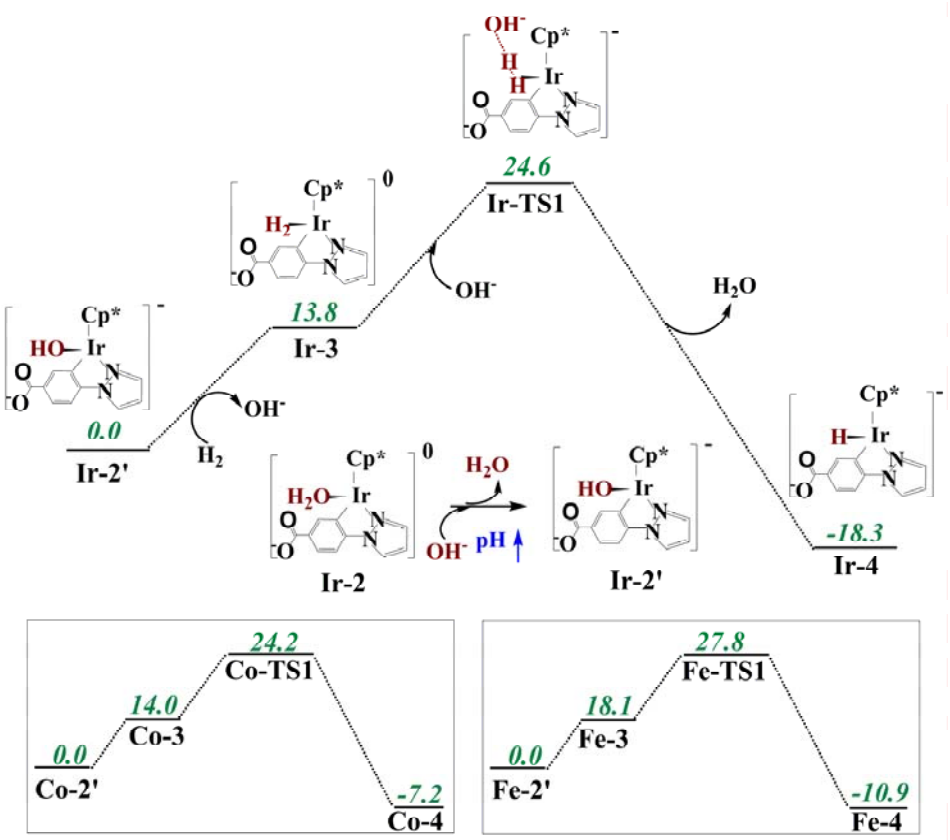

Figure 5. The free energy profiles (italic numbers in kcal/mol) for the reaction of **M-2′** (**Ir-2′**, **Co-2′**, and **Fe-2′**) with dihydrogen to afford iridium hydride complex **M-4** (**Ir-4**, **Co-4**, and **Fe-4**) in basic solution.

3.2.2 Hydrogenation of both carbon dioxide and hydrogen carbonate (HCO_3^-)

After the formation of the metal-H species **M-4** with high reduction activity, it is likely to hydrogenate either carbon dioxide or hydrogen carbonate. Firstly, we discuss the hydrogenation of carbon dioxide. Free molecular CO_2 firstly approaches to the H

atom of M-H bond by H-bond interaction to generate the complex **M-5** with the free energy absorbing of 6.1 kcal/mol, 5.6 kcal/mol, and 6.3 kcal/mol for Ir, Co, and Fe, respectively. Subsequently, transition sate **M-TS2** describes a direct outer-sphere transfer of the metal-hydride to C atom of CO_2 without the structural change of the [C, N] chelating ligand (see Figure 6). The favorable activation free energy barriers ($\Delta G^{\ddagger}$) were calculated to be 8.5 kcal/mol, 9.6 kcal/mol, and 5.0 kcal/mol for **Ir-TS2**, **Co-TS2**, and **Fe-TS2**, respectively, indicating the kinetically advantage for the formation of formate complex **M-6**. As shown in Figure 6, the transition state **M-TS2** structure is stabilized by two weak hydrogen bonding interactions with the Cp* hydrogen atoms. A hydrogen bond-stabilized transition state usually gives access to facile hydride transfer for a formate complex. Except for the advantage in structure, the highly activity of the transfer hydrogenation may be ascribed to the strong election-donating ability of oxyanion on $–COO^-$ group. We give the detailed analysis in the following cycle II. For hydrogen metal-H transfers to CO_2, another usual mechanism is inner-sphere mechanism that involves the precoordination of CO_2 to the metal center. The analogous inner-sphere transition state in cycle II was located (vide infra), where the Ir-N bond break of the [C, N] chelating coordination for providing vacant site needs the highly energy consuming. Thus, we view the present catalytic system should follow the low-barrier outer-sphere mechanism rather than inner-sphere mechanism with serious structural changing.[23] The resulting formate complex **M-6** has a coordination mode involving the one terminal oxygen atom. For the iridium model, the activation barrier from **Ir-4** to **Ir-TS2** is 8.5 kcal/mol, which is slightly

lower than 10.8 kcal/mol of dihydrogen heterolysis. However, the formation of the formate complex **Ir-6** is slower than metal-hydride complex **Ir-4** in experiment. Notice, for the formation of **Ir-6**, the lower 5.1 kcal/mol reverse barrier is found to allow **Ir-6** to convert back to **Ir-4**. In addition, in order to regenerate the active catalyst **Ir-2**, the loss of the formate ligand accompanied by the coordination of water is 6.7 kcal/mol uphill, which further facilitate the reverse reaction. On the other hand, the formation of **Ir-4** has a great thermodynamically advantage. Thus, we suggest both the considerable unfavorable thermodynamic natures and the kinetic activation barrier with less advantage are the reasons why the slower formation of the formate complex **Ir-6** in comparison with the hydride complex **Ir-4**. Interestingly, there is no competitive reverse reaction for both **Co** and **Fe** complex. The relatively stable formate intermediate **Co-6** and **Fe-6** leads to the relatively high reverse barrier, 14.6 kcal/mol and 14.0 kcal/mol for **Co** and **Fe**, respectively. Overall, stabilization of the formation of formic acid from hydrogen and carbon dioxide is 24.5 kcal/mol, so the hydrogen storage is thermodynamically significantly favorable.

In view of hydrogenation of hydrogen carbonate provided by experiment, we explored that the hydride Ir-H transfers to C atom of hydrogen carbonate substrate followed by the leaving of the OH^- moiety to give formate complex **Ir-6**. However, the outer-sphere direct hydrogen transfer transition state similar to **Ir-TS2** was not located. Our multi-optimizations all give transition state **Ir-TS3,** where the Ir-N bond is broken ($d_{Ir\text{-}N}$=4.569 Å) to give vacant site for the coordination of HCO_3^- to Ir center ($d_{Ir\text{-}O}$=2.058 Å), simultaneously, the hydridic H1 transfers to C1 of HCO_3^- from Ir

metal ($d_{Ir\text{-}H1}$=2.352 Å and $d_{H1\text{-}C1}$=1.180 Å). Subsequently, the leaving of the OH^- moiety occurs via transition state **Ir-TS4** with the lengthen C1-O2 bond ($d_{C1\text{-}O2}$=2.207 Å) and the shorten Ir-O1 bond ($d_{Ir\text{-}O1}$=1.996 Å). Unfortunately, the reaction activation barriers for the formation of formate from HCO_3- are substantially high, 34.5 kcal/mol for **Ir-TS3** and 21.3 kcal/mol **Ir-TS4**, relative to metal-hydride complex **Ir-4**. Therefore, it was confirmed that the hydridic ligand of **Ir-4** is abstracted by CO_2 rather than bicarbonate (HCO_3^-) to produce formate at pH 8.8 in experiment. So it is necessary that the bicarbonate decomposes to carbon dioxide ($HCO_3^- \rightarrow CO_2+OH^-$) in real reaction process. The decomposition of bicarbonate has the 20.4 kcal/mol reaction energy and is believed to be the rate-determining step of hydrogen storage cycle, because this energy consuming is higher than energy barrier of either H_2 heterolysis or hydrogenation of carbon dioxide. In addition, this endergonic decomposition reaction may be another important reason why the formation of the formate complex **Ir-6** is slower than hydride complex **Ir-4** in experiment.

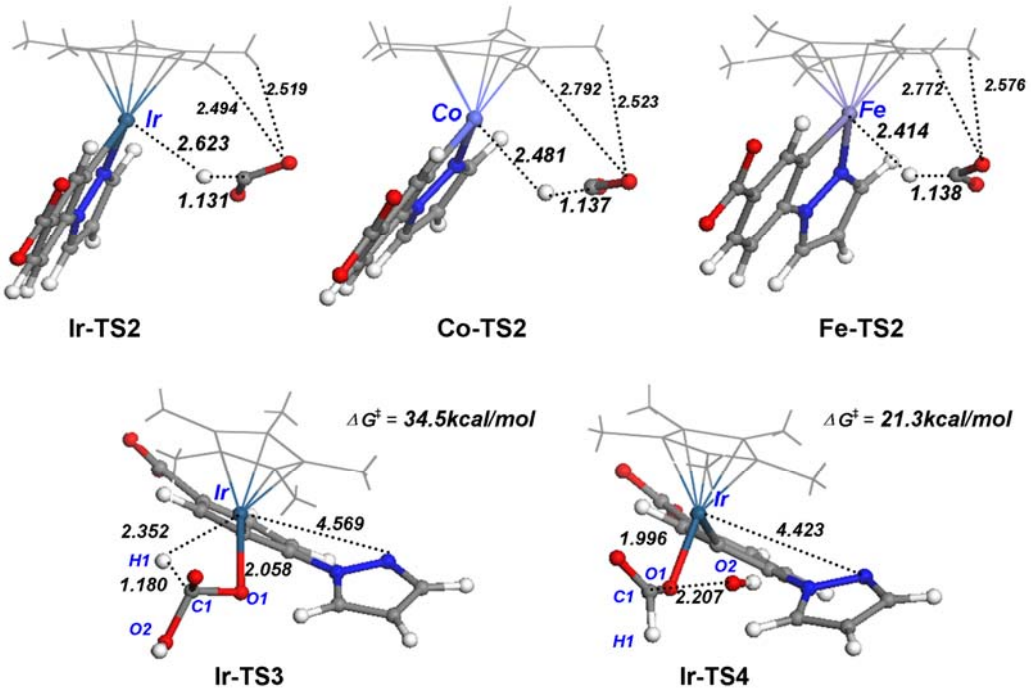

Figure 6. The optimized transition states structures (bond length/Å) for hydrogenation of both carbon dioxide and hydrogen carbonate (HCO_3^-). [24]

3.3 Hydrogen evolution

For hydrogen evolution catalytic cycle II in acid solution, overall mechanism illustration is presented in scheme 3, the free energy profiles are shown in Figures 7 and 9, and the corresponding key optimized structures are given in Figures 8 and 10.

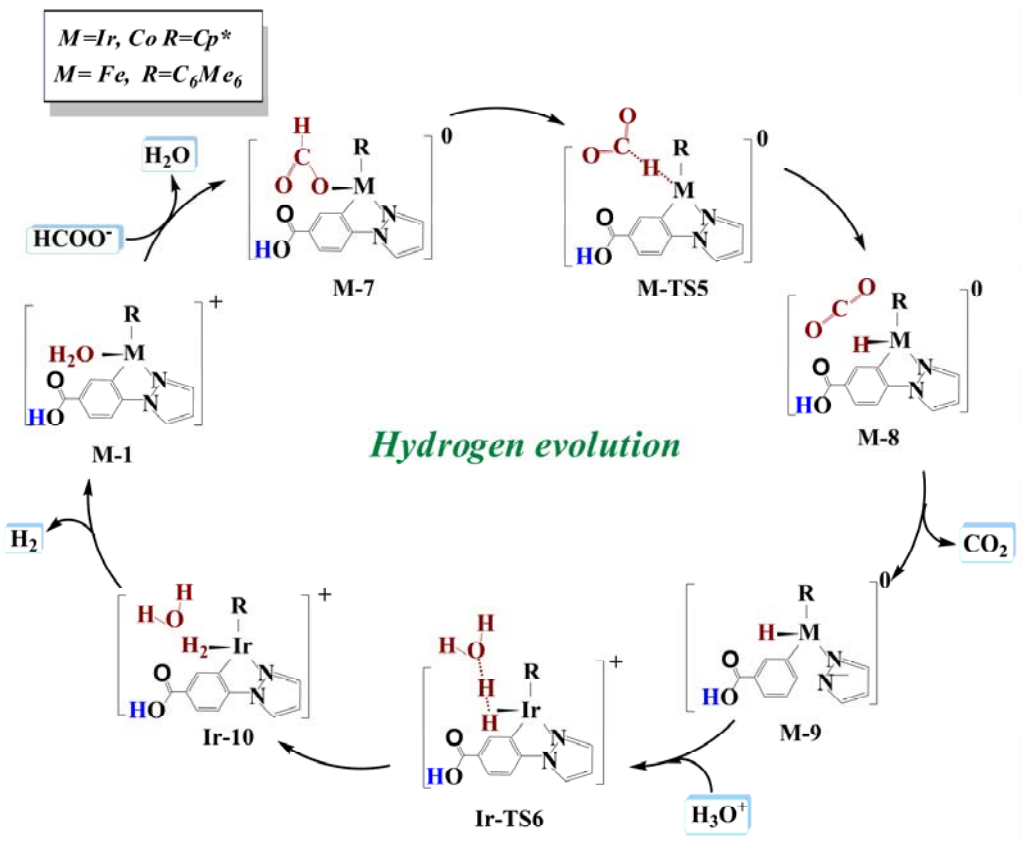

Scheme 3. Overall mechanism schematic illustration for the hydrogen evolution in acid solution (*Cycle II*).

3.3.1 The *β*-hydride elimination of formate

Under pH=2.8 acidic experimental condition, the active catalyst **M-1** for hydrogen evolution is formed from the active hydrogen storage catalyst **M-2** by the protonation of oxyanion (scheme 1). As shown in scheme 3, the water ligand of the active catalyst **M-1** was firstly exchanged for the noncoordinating formate anion to form formate complex **M-7**. Subsequently, the *β*-hydride of formate will transfer to metal center via outer-sphere transition state **M-TS5** to give iridium-hydride intermediate **M-8**. The mechanism of *β*-hydride transfer could be either intermolecular (outer-sphere mechanism), with hydride transfer from an unbound formate molecule to the metal, or intramolecular (inner-sphere mechanism), with

hydride transfer to metal center from a formate ligand. As shown in Figure 8, transition state **Ir-TS5** involves the *β*-hydrogen transfer of noncoordinating formate anion to center Ir in the second coordination sphere, leading to intermediate **Ir-8** with metal-H bond and straight line CO_2 molecule. The active barriers from **Ir-7** to **Ir-TS5** are 19.3 kcal/mol, which is in well agreement with experimental result, 18.9 kcal/mol. Transition states **Co-TS6** and **Fe-TS6** comparatively have the lower active barriers, 14.1 kcal/mol and 12.8 kcal/mol, respectively. On the other hand, transition state **Ir-TS5′** describes the *β*-H elimination of the coordinated formate with the $\Delta G^{\ddagger}$=25.6 kcal/mol. This reaction manner needs the breaking Ir-N bond to provide vacant site for the *β*-H elimination. Obviously, the highly active barrier of the inner-sphere mechanism is not favorable, which may be ascribed to the serious structural changing involving the break of Ir-N coordination bond. Therefore, the outer-sphere *β*-H elimination is believed to be the feasible mechanism for the C-H bond cleavage in hydrogen evolution cycle. Notice that herein the reverse reaction of formate *β*-H elimination (**Ir-9→Ir-TS5→Ir-7**) is similar to hydrogen abstraction by CO_2 (**Ir-4→Ir-TS2→Ir-6**) in hydrogen storage, the benzoic acid moiety of complex **Ir-9** undergoes deprotonation to form the benzoate complex **Ir-4**. However, the activation barrier of the former, 23.9 kcal/mol, is considerable higher than that of the latter, 8.5 kcal/mol. In **Ir-4**, the pendent base with strong electron-donating ability may significantly facilitate hydrogen Ir-H transfers to free CO_2. The charge distribution of **Ir-4** and **Ir-9** are shown in Table 2, the negative charge of [C,N] ligand (-1.642 e) is larger for **Ir-4** as compared to **Ir-9** (-0.999 e). The HOMO level of **Ir-4** (-0.198 e) is

slightly higher than that of **Ir-9** (-0.203 e), indicating the stronger donor capability of the former than the latter. Moreover, the Ir-H moiety of **Ir-4** (1.268 e) has the stronger hydridic (nucleophilicity) character as compared to **Ir-9** (1.443 e), which can facilitate the metal hydride transfer toward the carbonyl group of CO_2. Therefore, the acid-base equilibrium of catalyst [C, N] ligand controlled by varying the solution pH can effectively provide a desirable catalytic activity for the present catalytic system, i.e., in the hydrogen storage process, the important dehydrogenation by CO_2 is activated, while in the hydrogen evolution process, the reverse reaction of the key β-H elimination is prevented. The pronounced enhancement of catalytic efficiency is provided to both catalytic cycles by adjusting pH in solution.

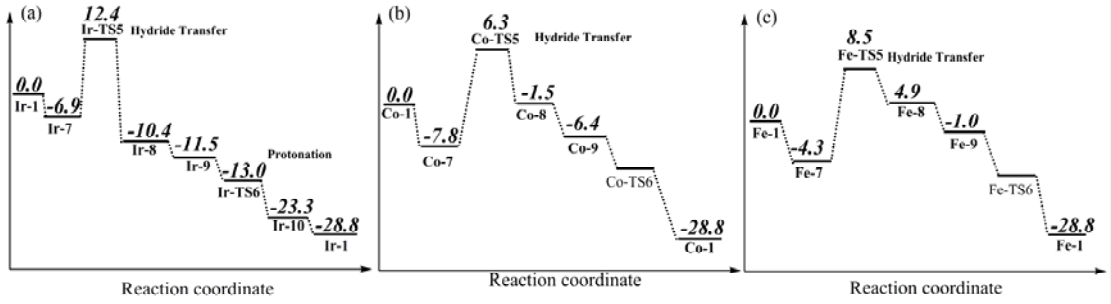

Figure 7. The free energy (italic numbers in kcal/mol) profiles for the hydrogen evolution catalyzed by Ir-1 (a), Co-1 (b), and Fe-1 (c).

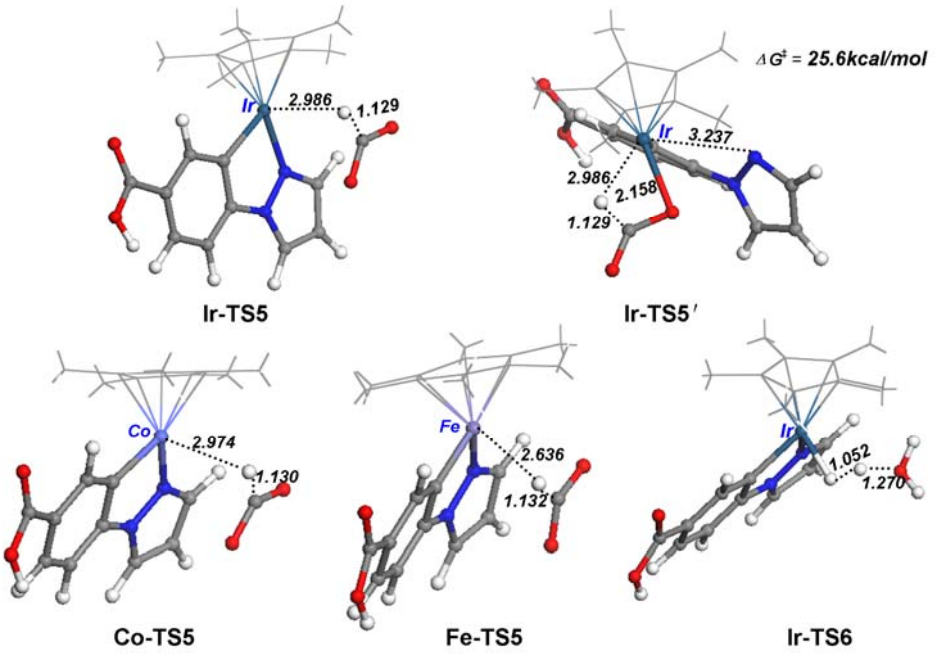

Figure 8. The optimized transition sates structures (bond length/Å) involved in Figure 7.

Table 2. HOMO level and charge distribution of **Ir-4** and **Ir-9** calculated at the M06/BSII (SMD) level.

Complex	HOMO Level (ev)	Charge Ir-H	Charge [C,N] ligand	Charge Cp*
Ir-4	-0.198	1.268	-1.642	-0.576
Ir-9	-0.203	1.443	-0.999	-0.444

3.3.2 The protonation of metal-hydride bond

As shown in Figure 8, transition state **Ir-TS6** describes a dihydrogen bond interaction between a hydride Ir-H of **Ir-9** and hydrated proton H_3O^+ in the second coordination sphere ($d_{H\text{-}H}$=1.052 Å and $d_{H\text{-}O}$=1.270 Å). The protonation of the Ir-H bond leads to the formation of a dihydrogen bonded complex **Ir-10**. As shown in Figure 7, the process from **Ir-9** to **Ir-10** monotonically decreases without barrier, indicating the easy protonation process. Finally, the readily release of H_2 takes place

upon the attack by solvent H_2O on the metal center to regenerate active catalyst **Ir-1**. Unfortunately, although the multi-attempting were performed, transition states **Co-TS6** and **Fe-TS6** analogous to **Ir-TS6** were still not located. As shown in Table 3, compared to NBO charge on hydride Ir-H of **Ir-9**, 0.064 e, the hydrogen atoms of both Co-H of **Co-9** and Fe-H of **Fe-9** have less hydridic character, 0.161 e and 0.168 e, respectively, so electrostatic repulsion with the positively charged proton of the approaching H_3O^+ is likely to obstacle the formation of transition states **Co-TS6** and **Fe-TS6.** Interestingly, we found the other possible low-energy reaction manner for Co and Fe complexes, free energy profile and the key optimized structures are presented in Figures 9 and 10, respectively. When the H_3O^+ approaches the C atom of Ir-C coordination bond of intermediate **Co-9** (**Fe-9**), the protonation will occur accompanied by the weakened Ir-C coordination bond ($d_{Co\text{-}C}$=2.330 Å and $d_{Fe\text{-}C}$=2.272 Å) to give the stable intermediate **Co-10** (**Fe-10**). Subsequently, the more stable intermediate **Co-11** (**Fe-11**) is formed with the release of H_2O. Then, transition sate **Co-TS7** (**Fe-TS7**) describes that the hydride of the new C-H bond transfers to hydride metal-H (Co: $d_{C\text{-}H}$=1.454 Å and Fe: $d_{C\text{-}H}$=1.412 Å) with the recovery of the metal-C bond ($d_{Co\text{-}C}$=1.989 Å and $d_{Fe\text{-}C}$=2.080 Å) to afford intermediate **Co-12** (**Fe-12)** with the dihydrogen ligand. Finally, the ligand exchange between H_2 and H_2O easily occurs to regenerate the initial active catalyst **Co-1(Fe-1)**. The activation barriers of this kind of protonation process are 5.8 kcal/mol and 2.0 kcal/mol for Fe and Co, respectively, which are low enough to accept.

Table 3. The NBO charges on the metal H atom of complexes **Ir-9**, **Co-9**, and **Fe-9** calculated at the M06/BSII level.

Complex	Ir-9	Co-9	Fe-9
Metal H	0.064	0.161	0.168

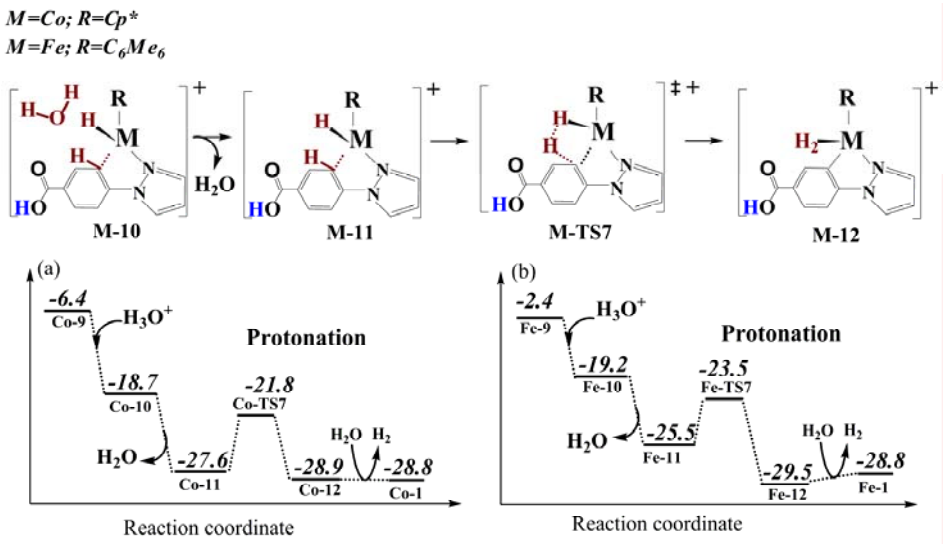

Figure 9. The free energy (italic numbers in kcal/mol) profiles for the protonation processes in Co-catalyzed (a) and Fe-catalyzed (b) hydrogen evolution cycles.

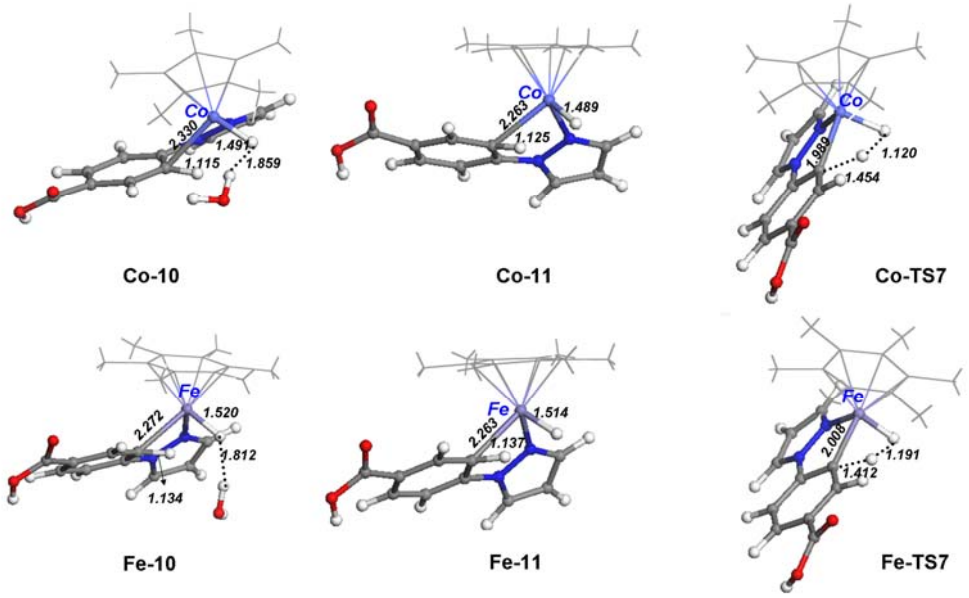

Figure 10. The optimized structures (bond length/Å) of the key intermediates and transition sates involved in Figure 9.

3.4 High-spin state cases of Co and Fe models

3.4.1 Co model

We ruled out the cases of the high-spin states for Co metal model. As shown in Figure 11, compared to the singlet state catalysts **Co-1** and **Co-2**, triplet sate catalysts **3-Co-1** and **3-Co-2** are 15.0 kcal/mol and 2.1 kcal/mol higher in free energy while quintet state catalysts **5-Co-1** and **5-Co-2** 9.1 kcal/mol and 9.0 kcal/mol higher, respectively. In addition, both the Cp* of **5-Co-1** and the hexamethylbenzene of **5-Co-2** have been converted to η^2-coordiantion from η^5-coordiantion. The decoordination usually occur when the saturated structures are optimized in the high-spin states.

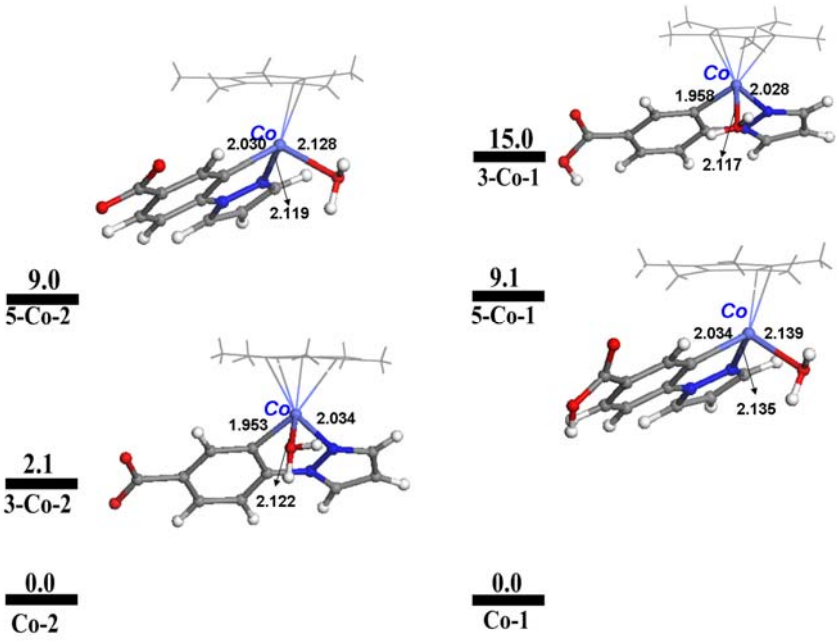

Figure 11. For both quintet and triplet states of active catalysts **Co-1** and **Co-2** in Co model, the free energies relative to single state (kcal/mol) and optimized structures (bond length/Å).

3.4.2 Fe model

As shown in Figure 12, opposite to Co model, the lower free energies are found for both triplet and quintet states of active catalysts **Fe-1** and **Fe-2** in Fe model. On the one hand, the triplet-state catalysts **3-Fe-1** and **3-Fe-2** are 18.6 kcal/mol and 16.0 kcal/mol lower in free energy, which directly leads to the activation barriers of 25.2 and 27.1 kcal/mol in hydrogen storage and evolution, respectively (see red font in Figure 12). On the other hand, the quintet-state catalysts **5-Fe-1** and **5-Fe-2** are 41.7 kcal/mol and 43.4 kcal/mol considerable lower, respectively. Moreover, the geometrical structural results show that the hexamethylbenzene ligands in quintet-state case have completely dissociated from the Fe center (see Figure 12). In addition, we also explored the possible triplet reaction pathways following the **3-Fe-2** and **3-Fe-1**. However, followed by **3-Fe-2**, the optimized structure of triplet state intermediate **3-Fe-3** in Figure 12 indicates that dihydrogen can not coordinate to metal center when the initial ligand exchange between H_2 with H_2O occurs. The Co model has the similar situation. Followed by **3-Fe-1**, Even if multi-optimizations were performed, but the triplet state transition state **3-Fe-TS5** associated with **Fe-TS5** was still not located. Likely, the formate ligand trends to leave away from metal center during the optimization process. As mentioned above, the decoordination usually occur when the saturated structures are optimized in the high-spin states. Noticeably, it should be difficult to prepare the singlet-state Fe-complex because the quintet and triplet states of active catalysts **Fe-1** and **Fe-2** are much lower than the singlet states. Therefore, the presence of low-energy high-spin states of active catalysts may

obstacle the smooth proceeding of the catalytic reaction in Fe-model.

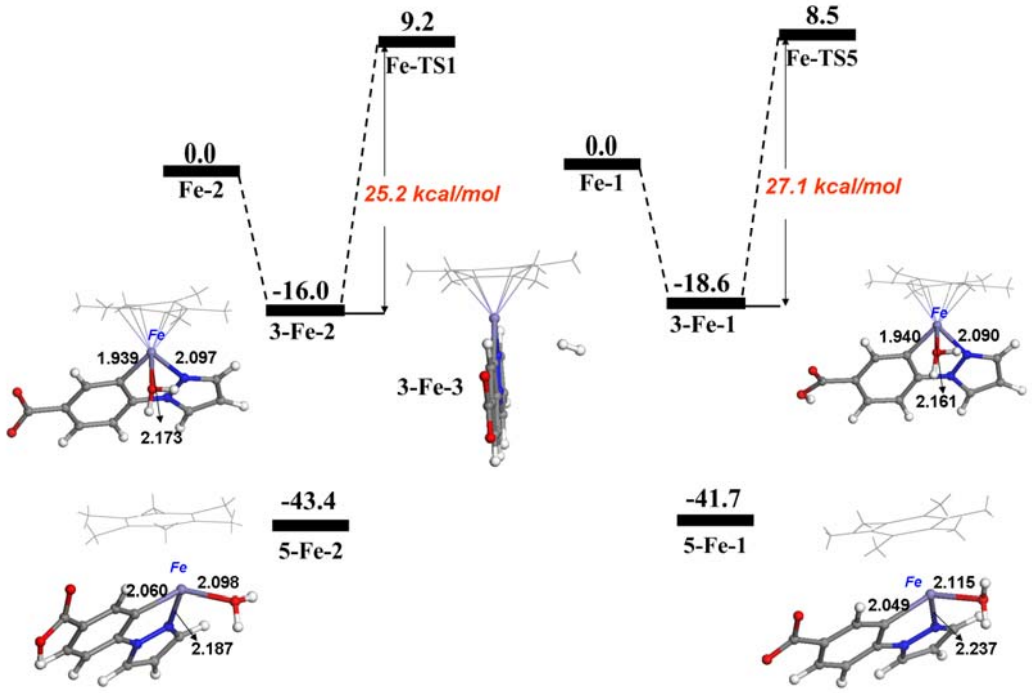

Figure 12. For both quintet and triplet states for active catalysts Fe-1 and Fe-2 in Fe model, the free energies relative to single state (kcal/mol) and optimized structures (bond length/Å).

4. Conclusion

Herein, we report the detailed reaction mechanism studies for interconversion between H_2 and HCOOH catalyzed by [C,N] cyclometalated organoiridium complex using the density functional theory (DFT) calculations. The hydrogen storage catalytic cycle (cycle I) is consisted of four stages: (stage I) the ligand exchange of H_2O by H_2, (stage II) the H_2 heterolysis cleavage facilitated by OH^- to give the extremely stable metal hydrido intermediate **Ir-4**, (stage III) the hydrogen Ir-H tranfer to CO_2 via direct outer-sphere hydride transfer to give the formate complex, (stage IV) the exchange of formate ligand by water to regenerate active catalyst **Ir-2**. Among, the decomposition

of bicarbonate to CO_2 in stage III is believed to the rate-determining step for hydrogen storage cycle with 20.4 kcal/mol energy absorbing. In addition, the stage III is the key reaction step because the reverse reaction is significantly easy to occur. On the other hand, the catalytic cycle II for H_2 evolution also involves four stages, (stage I) anion $HCOO^-$ replace the water ligand of the cationic aqua complex **Ir-1** to afford the corresponding formate complex, (stage II) the formation of iridium hydrido complex **Ir-9** via outer-sphere *β*-H elimination mechanism of the formate, (stage III) The protonation of the hydrido Ir-H by H_3O^+ to produce H_2 in iridium center, (stage IV) the release of H_2 to recover active catalyst **Ir-1**. In cycle II, the *β*-H elimination of formate with 19.3 kcal/mol activation barrier is believed to the rate-determining step, which is in well agreement with the experimental result. Our calculations show that the role of the pH adjusting in the catalytic system is mainly represented in two aspects: the one aspect is the direct participation of ions OH^- and H_3O^+ in catalytic reaction step, that is, the former assists the H_2 heterolysis in cycle I while the latter protonates metal-hydrido complex in cycle II; the other aspect is that the acid-base equilibrium of catalyst [C, N] ligand controlled by varying the solution pH can affect hydrogen transfer, that is, the pendent base with strong electron-donating ability facilitate the metal H transfer to CO_2 in cycle I. In addition, our calculation show the structural changing of the [C,N] bidentate ligand generally induce the serious energy consuming, so unaltered [C,N] bidentate ligand should be necessary to the smooth going of the whole reaction. Our mechanism studies are well consistent with the experimental results and provide a precise interpretation of the observed experimental

behavior.

Our theoretical designed Co complex may be effective catalyst for the interconversion between formic acid and dihydrogen because it has the slightly lower activation barriers for both catalytic cycle I and II in comparison with the case of Ir-complex. However, for Fe complex, the low-energy triplet and quintet states of active catalysts **Fe-1** and **Fe-2** are unfavorable for the preparation of the singlet Fe-complex, so the smooth proceeding of the catalytic reaction may be negatively affected. Our studies on both Co and Fe complexes are essential for the development of new low-cost catalysts for the dihydrogen-formic acid Interconversion system. We hope the data provided in this paper will facilitate mechanistic studies of growing interestingly sustainable H_2 storage/delivery.

Acknowledgements

The authors thank the National Basic Research Program of China (973 Program; 2012CB932800), the National Natural Science Foundation of China (No.21303067, No.21373099) and Doctoral Fund of Ministry of Education of China (No.20130061110020) for financial support of this research.

Notes and References

1 A. Boddien, C. Federsel, P. Sponholz, D. Mellmann, R. Jackstell, H. Junge, G. Laurenczy and M. Beller, *Energy Environ. Sci.* 2012**, 5**, 8907.

2 (a) M. Czaun, A. Goeppert, J. Kothandaraman, R. B. May, R. Haiges, G. K. S. Prakash and G. A. Olah, *ACS Catal.* 2014**, 4**, 311; (b) B. Loges, A. Boddien, H. Junge and M. Beller, *Angew. Chem. Int. Ed.* 2008**, 47**, 3962; (c) A. Boddien, B. Loges, H. Junge and M. Beller, *ChemSusChem* 2008**, 1**, 751; (d) G. Centi, E. A. Quadrelli and S. Perathoner, *Energy Environ. Sci.* 2013**, 6**, 1711; (e) Y. Y. Cai, X. H.

Li, Y. N. Zhang, X. Wei, K. X. Wang and J. S. Chen, *Angew. Chem. Int. Ed.* 2013**, 52**, 11822.

3 (a) A. D. Getty, C.-C. Tai, J. C. Linehan, P. G. Jessop, M. M. Olmstead and A. L. Rheingold, *Organometallics* 2009**, 28**, 5466; (b) A. Urakawa, M. Iannuzzi, J. Hutter and A. Baiker, *Chem. Eur. J.* 2007**, 13**, 6828; (c) Siu M. Ng, C. Yin, Chi H. Yeung, Tak C. Chan and Chak P. Lau, *Eur. J. Inorg. Chem.* 2004**, 9**, 1788; (d) A. Urakawa, F. Jutz, G. Laurenczy and A. Baiker, *Chem. Eur. J.* 2007**, 13**, 3886; (e) F. Hutschka, A. Dedieu, M. Eichberger, R. Fornika and W. Leitner, *J. Am. Chem. Soc.* 1997**, 119**, 4432; (f) T. Matsubara, *Organometallics* 2001**, 20**, 19; (g) Y. Musashi and S. Sakaki, *J. Am. Chem. Soc.* 2002**, 124**, 7588; (h) Y. Musashi and S. Sakaki, *J. Am. Chem. Soc.* 2000**, 122**, 3867; (i) H. Ohtsu and K. Tanaka, *Angew. Chem. Int. Ed.* 2012**, 51**, 9792; (j) Y.-N. Li, L.-N. He, A.-H. Liu, X.-D. Lang, Z.-Z. Yang, B. Yu and C.-R. Luan, *Green Chem.* 2013**, 15**, 2825.

4 (a) Y. M. Badiei, W. H. Wang, J. F. Hull, D. J. Szalda, J. T. Muckerman, Y. Himeda and E. Fujita, *Inorg. Chem.* 2013**, 52**, 12576; (b) S. Sanz, A. Azua and E. Peris, *Dalton Trans* 2010**, 39**, 6339; (c) S. Sanz, M. Benítez and E. Peris, *Organometallics* 2010**, 29**, 275; (d) D. J. Morris, G. J. Clarkson and M. Wills, *Organometallics* 2009**, 28**, 4133; (e) W.-H. Wang, J. F. Hull, J. T. Muckerman, E. Fujita and Y. Himeda, *Energy Environ. Sci.* 2012**, 5**, 7923; (f) S. Ogo, R. Kabe, H. Hayashi, R. Harada and S. Fukuzumi, *Dalton Trans.* 2006**, 39**, 4657.

5 (a) M. A. Iron, E. Ben-Ari, R. Cohen and D. Milstein, *Dalton Trans* 2009, 9433; (b) T. J. Schmeier, G. E. Dobereiner, R. H. Crabtree and N. Hazari, *J. Am. Chem. Soc.* 2011**, 133**, 9274; (c) G. A. Filonenko, M. P. Conley, C. Copéret, M. Lutz, E. J. M. Hensen and E. A. Pidko, *ACS Catal.*2013**, 3**, 2522; (d) R. Tanaka, M. Yamashita and K. Nozaki, *J. Am. Chem. Soc.* 2009**, 131**, 14168; (e) C. Federsel, R. Jackstell and M. Beller, *Angew. Chem. Int. Ed.* 2010**, 49**, 6254.

6 Y. Himeda, N. Onozawa-Komatsuzaki, H. Sugihara and K. Kasuga, *Organometallics* 2007**, 26**, 702.

7 Y. Himeda, *Green Chemistry* 2009**, 11**, 2018.

8 Y. Himeda, *Eur. J. Inorg. Chem.* 2007**, 2007**, 3927.

9 (a) Y. Manaka, W. H. Wang, Y. Suna, H. Kambayashi, J. T. Muckerman, E. Fujita and Y. Himeda, *Catal. Sci. Technol.* 2014**, 4**, 34; (b) S. Fukuzumi, T. Kobayashi and T. Suenobu, *ChemSusChem* 2008**, 1**, 827; (c) C. Fellay, N. Yan, P. J. Dyson and G. Laurenczy, *Chem. Eur. J.* 2009**, 15**, 3752; (d) S. Oldenhof, B. de Bruin, M. Lutz, M. A. Siegler, F. W. Patureau, J. I. van der Vlugt and J. N. Reek, *Chem. Eur. J.* 2013**, 19**, 11507; (e) C. Fellay, P. J. Dyson and G. Laurenczy, *Angew. Chem. Int. Ed.* 2008**, 47**, 3966; (f) J. H. Barnard, C. Wang, N. G. Berry and J. Xiao, *Chem. Sci.* 2013**, 4**, 1234; (g) T. W. Myers and L. A. Berben, *Chem. Sci.* 2014**, 5**, 2771; (h) J. S. Yoo, F. Abild-Pedersen, J. K. Nørskov and F. Studt, *ACS Catal.* 2014**, 4**, 1226; (i) J. A. Herron, J. Scaranto, P. Ferrin, S. Li and M. Mavrikakis, *ACS Catal.* 2014**, 4**, 4434; (j) D. A. Bulushev, L. Jia, S. Beloshapkin and J. R. Ross, *Chem. Commun.* 2012**, 48**, 4184; (k) M. E. M. Berger, D. Assenbaum, N. Taccardi, E. Spiecker and P. Wasserscheid, *Green Chem.* 2011**, 13**, 1411.

10 R. Tanaka, M. Yamashita, L. W. Chung, K. Morokuma and K. Nozaki, *Organometallics* 2011**, 30**, 6742.

11 (a) Y. Maenaka, T. Suenobu and S. Fukuzumi, *Energy Environ. Sci.* 2012**, 5**, 7360; (b) S. Moret, P. J. Dyson and G. Laurenczy, *Dalton Trans.* 2013**, 42**, 4353; (c) S. Fukuzumi, T. Kobayashi and T. Suenobu, *J. Am. Chem. Soc.*2010**, 132**, 1496.

12 (a) R. H. Crabtree, *New J. Chem.* 2011**, 35**, 18; (b) J. Vijaya Sundar and V. Subramanian, *Organometallics* 2012**, 31**, 8525; (c) W.-H. Wang, J. T. Muckerman, E. Fujita and Y. Himeda, *ACS Catal.* 2013**, 3**, 856; (d) J. F. Hull, Y. Himeda, W.-H. Wang, B. Hashiguchi, R. Periana, D. J. Szalda, J. T. Muckerman and E. Fujita, *Nature Chemistry* 2012, 383.

13 M. S. G. Ahlquist, *Journal of Molecular Catalysis A: Chemical* 2010**, 324**, 3.

14 (a) Y.-y. Ohnishi, T. Matsunaga, Y. Nakao, H. Sato and S. Sakaki, *J. Am. Chem. Soc.* 2005**, 127**, 4021; (b) K. Muller, Y. Sun, A. Heimermann, F. Menges, G. Niedner-Schatteburg, C. van Wullen and W. R. Thiel, *Chemistry* 2013**, 19**, 7825.

15 (a) X. Yang, *Dalton Trans* 2013**, 42**, 11987; (b) R. Sanchez-de-Armas, L. Xue and M. S. Ahlquist, *Chem. Eur. J.* 2013**, 19**, 11869 ; (c) L. Yang, H. Wang, N. Zhang and S. Hong, *Dalton Trans.* 2013**, 42**, 11186; (d) C. Federsel, A. Boddien, R. Jackstell, R. Jennerjahn, P. J. Dyson, R. Scopelliti, G. Laurenczy and M. Beller, *Angew. Chem. Int. Ed.* 2010**, 49**, 9777; (e) A. Boddien, D. Mellmann, F. Gartner, R. Jackstell, H. Junge, P. J. Dyson, G. Laurenczy, R. Ludwig and M. Beller, *Science* 2011**, 333**, 1733; (f) A. Boddien, B. Loges, F. G. rtner, C. Torborg, K. Fumino, H. Junge, Ralf Ludwig and M. Beller, *J. Am. Chem. Soc.* 2010**, 132**, 8924; (g) C. Ziebart, C. Federsel, P. Anbarasan, R. Jackstell, W. Baumann, A. Spannenberg and M. Beller, *J. Am. Chem. Soc.* 2012**, 134**, 20701; (h) R. Langer, Y. Diskin-Posner, G. Leitus, L. J. Shimon, Y. Ben-David and D. Milstein, *Angew. Chem. Int. Ed.* 2011**, 50**, 9948.

16 M. S. Jeletic, M. T. Mock, A. M. Appel and J. C. Linehan, *J. Am. Chem. Soc.* 2013**, 135**, 11533.

17 (a) C. Federsel, C. Ziebart, R. Jackstell, W. Baumann and M. Beller, *Chem. Eur. J.* 2012**, 18**, 72; (b) X. Yang, *ACS Catal.* 2011**, 1**, 849.

18 M. J.Frisch, G. W. Trucks, H. B. Schlegel, G. E. Scuseria, M. A. Robb, J. R. Cheeseman, G. Scalmani, V. Barone, B. Mennucci, G. A. Petersson, H. Nakatsuji, M. Caricato, X. Li, H. P. Hratchian, A. F. Izmaylov, J. Bloino, G. Zheng, J. L. Sonnenberg, M. Hada, M. Ehara, K. Toyota, R. Fukuda, J. Hasegawa, M. Ishida, T. Nakajima, Y. Honda, O. Kitao, H. Nakai, T. Vreven, J. A. Montgomery, Jr., J. E. Peralta, F. Ogliaro, M. Bearpark, J. J. Heyd, E. Brothers, K. N. Kudin, V. N. Staroverov, R. Kobayashi, J. Normand, K. Raghavachari, A. Rendell, J. C. Burant, S. S. Iyengar, J. Tomasi, M. Cossi, N. Rega, J. M. Millam, M. Klene, J. E. Knox, J. B. Cross, V. Bakken, C. Adamo, J. Jaramillo, R. Gomperts, R. E. Stratmann, O. Yazyev, A. J. Austin, R. Cammi, C. Pomelli, J. W. Ochterski, R. L. Martin, K. Morokuma, V. G. Zakrzewski, G. A. Voth, P. Salvador, J. J. Dannenberg, S. Dapprich, A. D. Daniels, O. Farkas, J. B. Foresman, J. V. Ortiz, J. Cioslowski,and D. J. Fox, *Gaussian 09; revision A.02; Gaussian, Inc.: Wallingford, CT,2009.*

19 (a) A. D. Kulkarni and D. G. Truhlar, *J. Chem. Theory Comput.* 2011**, 7**, 2325; (b) Y. Zhao, N. E. Schultz and D. G. Truhlar, *J. Chem. Phys.* 2005**, 123**, 161103; (c) R. Valero, R. Costa, P. R. M. I. de, D. G. Truhlar and F. Illas, *J.Chem. Phys.* 2008**, 128**, 114103; (d) Y. Zhao and D. G. Truhlar, *J. Chem. Theory Comput.* 2009**, 5**, 324; (e) Y. Zhao and D. G. Truhlar, *Acc. Chem. Res.* 2008 **41**, 157; (f) C. J. Cramer and D. G. Truhlar, *Phys. Chem. Chem. Phys.* 2009**, 11**, 10757; (g) Y. Zhao and D. G. Truhlar, *Theor. Chem. Account.* 2007**, 120**, 215; (h) Y. Zhao and D. G. Truhlar, *J. Chem. Theory Comput.* 2011**, 7**, 669.

20 A. V., Marenich, C. J. Cramer and D. G. Truhlar, *J. Phys. Chem. B* 2009**, 113**, 6378.

21 D. H. Andrae, U., M. Dolg, H. Stoll and H. Preuss, *Theor. Chim. Acta.* 1990**, 77**, 123.

22 K. Fiukui, *Acc.Chem.Res.* 1981**, 14**, 368.

23 G. Manca, I. Mellone, F. Bertini, M. Peruzzini, L. Rosi, D. Mellmann, H. Junge, M. Beller, A. Ienco and L. Gonsalvi, *Organometallics* 2013**, 32**, 7053.

24 (a) G. Kovács, G. Schubert, F. Joó and I. Pápai, *Catalysis Today* 2006**, 115**, 53; (b) A. Boddien, F. Gartner, C. Federsel, P. Sponholz, D. Mellmann, R. Jackstell, H. Junge and M. Beller, *Angew. Chem. Int. Ed.* 2011**, 50**, 6411.